JCSE The Journal of Corrosion Science and Engineering
ISSN 1466-8858 Volume 12, Preprint 6 submitted 7 February 2009

Effect of Nano-Precipitates of Al (Sc_{x-1} Zr_x) on the Mechanical and Corrosion Behavior of Al-2.5 Mg Alloys in Neutral Chloride Solution

Zaki Ahmad[1], and B. J. Abdul Aleem[2]

ABSTRACT

Microanalytical, mechanical and electrochemical studies were undertaken to investigate the effect of nano-precipitates of Al(Sc_{x-1} Zr_x) on the mechanical and corrosion characteristics of Al-Mg 2.5 alloys containing 0,0.15, 0.3, 0.6, and 0.9% of Sc with 0.14% Zr. Addition of 0.3% Sc significantly increased the yield strength due to small precipitate sizes (5–19 nm) and high coherency and volume fraction of the nano-precipitates. An increase from 0.6% Sc to 0.9% decreased the yield strength. Largest contributor to the strength was grain boundary strengthening caused by pinning of grain boundary by precipitates. The alloys showed a good resistance to 3.5 wt% neutral chloride solution. Electrochemical parameters indicated high passivation tendency of the alloys because of highly coherent Al(Sc_{x-1} Zr_x) precipitates. The precipitates matrix interface and the secondary phase particles of copper were the preferred sites for corrosion initiation.

Keywords

Al-Mg alloys, electrochemical corrosion, strengthening, nano-precipitates, scandium, zirconium.

Abbreviations

FEG – Field Extrusion Gun
STEM – Scanning Transmission Electron Microscope
HRTEM – High-resolution Transmission Electron Microscope

[1] Professor, Mechanical Engineering Department, KFUPM, Dhahran 31261, Saudi Arabia, email: ahmadz@kfupm.edu.sa.
[2] **Corresponding Author**: Mechanical Engineering Department, KFUPM, Dhahran 31261, Saudi Arabia, email: abaleem@kfupm.edu.sa.

ISSN 1466-8858 Volume 12, Preprint 6 submitted 7 February 2009

INTRODUCTION

In the past decade researchers have shown a keen interest in the fabrication of ultra-fine grained aluminum alloys because they offer some advantages by improving mechanical and physical properties which may be exploited in industrial applications [1]. Attempts have been made to develop non-age hardenable systems with thermodynamically stable precipitates for high temperature strength, such as Al-Fe-V-Si alloys [2, 3].

The creation of coherent ultra-fine precipitates thermodynamically with an ordered Li_2 structure is essential to bring about significant improvements in high temperature mechanical strength, inhibition, and recrystallization in aluminum alloys. Al-Mg-Sc alloys have been developed in recent years with the purpose of improving the service properties of non-heat treatable Al-Mg Alloys [4].

Scandium can increase the recrystallization temperature of aluminum alloys up to 600°C, which is well above the solution heat temperature of all heat treatable aluminum alloys. The synergistic combination of Sc and Zr is most effective in inhibition of recrystallization. Scandium is a unique alloy addition because it form an equilibrium thermally stable Li_2 (Al_3Sc) phase with aluminum. The lattice parameter of Al_3Sc phase 0.410 nm [5] matches very well with aluminum matrix (0.405 nm) which reduces the driving force for coarsening of Al_3Sc particles. Al_3Sc precipitates are coherent with the matrix and contribute to the alloy strength by pinning of grain boundaries.

Addition of zirconium reduces coarsening kinetic and form metastable Li_2 Al_3Sc precipitate and hence it may be substituted for Sc to form $Al_3(Sc_{1-x}\ Zr_x)$ precipitates. Addition of zirconium and scandium increase the tensile strength over Zr-free alloys by pinning of grain boundaries by highly stable $Al_3(Sc_{1-x}\ Zr_x)$ precipitates [6–8]. Whereas studies have been

ISSN 1466-8858 Volume 12, Preprint 6 submitted 7 February 2009

conducted to find a correlation between the microstructure and mechanical properties of Al-Mg alloys alloyed with Sc and Zr, the evidence is inconclusive [9–11].

Similar attempts have not been made to find a correlation between the microstructure and corrosion resistance of these alloys. A major limitation was the easy access to equipment like HRTEM (high-resolution transmission electron microscope), FEGSTEM (field emission transmission electron microscope), and advanced analytical systems required to study the precipitates in the nanometer range.

The objective of the studies undertaken was to investigate the effect of the nano-sized $Al_3(Sc_{1-x}\ Zr_x)$ precipitates on corrosion resistance of Al-2.5 Mg alloy and to find a correlation between nano-precipitates, mechanical properties, and corrosion resistance of the alloys investigated.

EXPERIMENTAL

Materials

Aluminum alloy 5052 was doped with 0.1, 0.3, 0.6, 0.9 Sc, and 0.14 wt% Zr. The alloys were custom made by HYDRO, Germany. Dopants were added by melting in a recrystallized aluminum crucible under an argon atmosphere. Alloying was achieved in accordance with the guidelines of HYDRO, Germany. The dopants was covered by a foil of pure aluminum to protect from air contact and dipped in melt covered by argon. The alloy was chilled-cast in a copper mold. Strips of 2 mm thickness were obtained by an extrusion process. The chemical composition of the alloy is given in Table 1.

Experimental Studies

The specimens for tensile tests were machined from flat strips. Coolants were used during machining to avoid thermal degradation. All tensile tests were made according to ASTM Specification D638 [12], with a diameter of 5 mm and length of 25 mm. Instron 8801 was

ISSN 1466-8858 Volume 12, Preprint 6 submitted 7 February 2009

employed to perform all tensile tests at room temperatures. It is a closed loop servo-hydraulic single axis testing system. The machine was also equipped with a hydraulically actuated self-aligning gripping system and an extensometer (MFA). The tests were carried out at a constant strain rate of 10^{-4} s^{-1}.

Corrosion Tests

a) *Polarization Measurements*

All cyclic potentiodynamic polarization measurements were made in accordance with ASTM Standard practice G5-87 [13]. The specimen was polarized for one hour at –800 mV with respect to a saturated calomel electrode in 3.5 wt% NaCl. Polarization was commenced after 30 minutes of exposure and saturating the electrolyte with nitrogen. Polarization was commenced at a scan rate of 10 mV/mm from the corrosion potential and continued in the noble direction until a sharp rise in the current indicating the onset of potential (E_p) was observed. The scan was reversed after a pre-determined current value and continued in the reverse direction until it dropped to a low value. The protection potential (E_{pp}) was determined by the intersection of the reverse anodic polarization curve with the forward anodic polarization curve.

Specimen of alloys measuring 15 mm in diameter were used in the above experiment. They were polished with 320, 400, and 600 μm grit SiC paper using demineralized water as a lubricant. The specimen were washed with demineralized water and dried before exposure.

b) *Polarization Resistance*

Polarization resistance experiments were carried according to ASTM Standard G59-91 [14]. Polarization plots were obtained by applying a controlled potential scan over a potential range of ± 25 mV_{SCE} with respect to corrosion potential (E_{corr}) at a scanning rate of 1 mV/min. Constant β_a and β_c were determined from the Tafel plots. Specimens were exposed

ISSN 1466-8858 Volume 12, Preprint 6 submitted 7 February 2009

to nitrogen saturated 3.5 wt% NaCl for forty-five minutes prior to commencement of polarization.

c) *Structural Studies*

Thin foils of specimen were prepared by electropolishing in a 30% solution of HNO_3 and ethanol (–20°C) (15 V, 140 mA) using a double jet electropolisher. The specimens were examined by Techni T-20, S.Twin, and 3-D Quanta FEGSTEM. The optical system included field emission gun assembly with NG Schottky emitter source. The beam current was ≤ 200 mA, and the resolution 1.2 nm at 300 kV and 2.9 nm at 1 kV. Genesis SEM QUANT-ZAF software was used.

RESULTS AND DISCUSSIONS

Selected mechanical properties of Al-Mg alloys, with and without Sc, are shown in Table 2. The beneficial effect of scandium addition is clearly observed in the table. The yield strength of alloy 1 increased from 130 MPa to 255 MPa on addition of 0.3 wt% Sc. The results are principally in agreement with the previous results that each 0.1 wt% Sc addition causes an average increase of 50 MPa. The mechanical properties of alloys at room temperature are shown in Table 3. It is also observed that an increase in Sc contents from 0.15 to 0.3 increases the tensile strength and yield strength, however the incremental addition of 0.6 wt% to 0.9 wt% does not correspondingly increase the ultimate tensile and yield strengths, on the contrary a slight decrease in the above value is obtained. Zirconium contents in the experiments were constant (0.14 wt%).

The strengthening properties of Al-Mg-Sc-Zr alloys are reflected clearly at elevated temperatures when compared to the UTS and YS values (MPa) of an aluminum alloys. The UTS and YS of alloys containing 0.4 wt% Sc and 0.5 wt% Zr were twice and four times as high respectively as in alloy Al 6061-T6 [15]. The strength of Al-Mg-Sc can be further

ISSN 1466-8858 Volume 12, Preprint 6 submitted 17 February 2009

increased to levels of alloy Al 7075 by higher magnesium levels. Unfortunately, alloys containing higher Mg levels (6–10%) have posed serious processing problems and they are subjected to stress corrosion cracking [16]. The percent elongation of alloys decreases with higher concentrations of scandium and zirconium (Table 3). This is in confirmation with previous work done by the authors [17].

It was shown that aging for 200 hours at 561 K did not significantly effects the yield strength of alloy 3 which is in confirmation with a similar work done earlier [17]. It has been reported that n value of Sc added alloys were lower than Al-Mg alloys which is a behavior similar to that observed in Al-Li alloys [18].

The strengthening effect caused by Sc and Zr is the subject of extensive research. The effect of $Al_3(Sc_{x-1}, Zr_x)$ precipitates on the mechanical properties cannot be explained without extensive TEM studies because of the nano-metric size of the precipitates. Extensive HRTEM and FEGSTEM studies were, therefore, undertaken to explain the above observations on mechanical properties.

The strengthening effect of Al-Mg-Sc alloys depends mainly upon the size and coherency of the precipitates, composition, volume fraction, and pinning of grain boundaries by the precipitates. A FEGSTEM DF image of alloy containing 0.3 Sc and 0.15 Zr is shown in Figure 1. The sub-grains and coherent nano-precipitates are clearly observed in this figure. Another STEM image (Figure 2) shows the distribution of coherent nano-size precipitates. Both coarse and fine precipitates are shown in Figure 2. The grain boundary is clearly visible in the DF image (Figure 3). Dislocations at the sub-grain boundaries are observed in Figure 4. A high resolution TEM image shows the coherency of precipitates (Figure 5). Figure 6 shows a high resolution TEM image of grain boundary interface. Diffraction patterns of precipitates for five different sub-grains were analyzed. The EDAX analysis showed the

ISSN 1466-8858 Volume 12, Preprint 6 submitted 7 February 2009

presence of Al_3Sc fine precipitates (Figure 7). EDAX mapping of the alloy (0.3 SC, 0.15 Zr) shows the presence of Al-Sc_3 precipitates. The grain interior contained copper particles as shown in Figure 8. The pinning of dislocations and grain boundaries by precipitates of $Al(Sc_{x-1}\ Zr_x)$ is shown in Figure 9. The precipitate size ranged from 5 nm to 22 nm (Figure 10). The pinning by dislocation is the major contributor to the alloy strength as observed in our investigation. The grain boundary thickness was measured to be ~ 100 nm. A HRTEM image of alloy containing 0.6 Sc shows some precipitates homogeneously distributed (Figure 11). The precipitate size in the above alloy ranged from 19.4 to 56.7 nm (Figure 12). Small precipitate size, coherency, and their homogeneous distribution are pivotal to strengthening. Grain boundary interface and more dislocations are observed at the sub-grain boundaries than the grain interior (Figure 13). A higher volume fraction of coherent precipitates and lesser interfacial spacing is observed as shown by TEM studies. With higher scandium addition (0.9%) a larger number of coarse precipitates, dislocations, and the sub-grain boundaries are observed. The effect of $Al(Sc_{x-1}\ Zr_x)$ precipitates on the strengthening of Al-2.5 Mg alloys are in agreement with the strengthening theories accepted by most researchers [19]. However, studies on the kinetics of precipitates and growth of $Al_3(Sc, Zr)$ are seriously lacking. Alloys containing 0.3 to 0.6% Sc show higher strengths than alloys containing 0.9% Sc and 0.15% Sc as shown in Table 2. As shown by FEGSTEM micrographs the precipitate sizes in alloy containing 0.3% Sc are smaller (~ 5–19 nm) than the precipitate sizes in alloys containing 0.6% Sc (22–56 nm). The precipitates size is still higher with 0.9% Sc (70–75 nm). FEGSTM image of alloy containing 0.9% Sc is shown in Figures 14-a and 14.b. Dislocations at the grain boundaries are also observed. The above observations show that coherent $Al(Sc_{x-1}\ Zr_x)$ precipitates in the nanometric range contribute to the alloy strength through dislocation precipitation interaction. Magnesium addition synergistically assists in alloy strengthening by further reducing the mismatch between the lattice parameters [20]. The precipitate sizes in our findings range from 5 to 56 nm. However, it could not be ascertained what could be the optimum particle size to achieve maximum Orwan

ISSN 1466-8858 Volume 12, Preprint 6 submitted 7 February 2009

strengthening. The optimum particle size has an fundamental bearing on the strengthening mechanism.

Quantitative modeling work on the Area Phase Boundary (APB) and Orwan Model which link the particle size to the strength is scarce [20]. Fractures in the doped alloys occur in the ductile mode. A fractured surface showing dimples and river marks is shown in Figure 15. An enlarged image of fractured surface is shown in Figure 16. It is a universal opinion amongst research workers that pinning of the grain boundaries is the largest contributor to strengthening. Figure 9 show clearly the pinning of grain boundaries by the coherent precipitates. The evidence observed from yield strength, ductility, sub-grain size, volume of coherent particles, and yield stress data confirms the strengthening effect caused by small Sc and Zr addition. Also it is shown that scandium and zirconium addition create a significant effect on the strain hardening coefficient. Studies conducted earlier and the evidence presented in this work suggest that smaller addition of Sc and Zr to Al alloys makes the Al-Mg alloys highly attractive material for industrial applications. However, more research is needed to reach the level of strength of alloys Al-Mg with 10% Mg, or alloy 7075 which are subjected to stress corrosion cracking and used in aeronautical industry.

Corrosion Resistance of Al-Mg-Sc Alloys

The electrochemical behavior of pure aluminum and 6013 was determined in a previous study by the authors [21]. The I_{corr} values of pure aluminum and Al 6013-T4 were found to be 0.328 and 1.3 μA/cm^2 and the open circuit potential values as –850 mV_{SCE} and –650 mV_{SCE}, respectively. These values are relatively higher than those obtained for our experimental alloys. Table 4 shows the electrochemical parameters of scandium and zirconium added alloys. These values were obtained by polarization resistance measurements. The open circuit values shown are less active than alloy 5052 (alloys without

ISSN 1466-8858 Volume 12, Preprint 6 Submitted 7 February 2009

Zr and Sc addition). The E_{corr} of conventional alloys 6061-T6 and 6013-T4 is very close to pitting potential and they are subjected to pitting under freely corroding conditions.

Table 5 shows the electrochemical parameters of the alloys obtained after electrochemical cyclic polarization. In all stances E_{corr} is more negative to E_p (pitting potential), the difference between ($\Delta E = E_{corr} - E_{pit}$) value of the scandium alloys is not very significant and indicates the self-passivity tendency of these alloys. The passivity of Al-Mg-Sc-Zr alloys over the Al-Mg alloys is reported to be increased by 114% which shows the beneficial effect of Sc addition on the corrosion resistance.

As shown by Figures 16-a and 16-b, the preferred sites for localized corrosion are the interface between the intermetallic compounds and matrix, agglomerate of precipitates, and secondary phase particles of Cu. The EDS spectrum of the corroded alloy surface shows abundance of copper particles in the different zones marked 1, 2, and 3 in Figure 17-a. The EDS spectra of a copper-rich site are shown in Figure 17-b. The white particles were detected to be Cu particles. Figure 18 shows the breakdown of the oxide film (right corner). The formation of protective oxides is the key for corrosion resistance of Al-Mg alloys. The reaction at the metal-electrode interface proceeds by the reduction of oxygen and the formation of hydrated oxide as represented by Al_2O_3, nH_2O. These films are not soluble in neutral chloride solution. It has been suggested that the formation of Al_3Sc increases the concentration of vacancies and partially oxides with oxygen to form Sc_2O_3 which deposits on the surface. The thermodynamic activity of aluminum promotes the formation of a less defective layer of aluminum oxy-hydroxides, such as bayerites and boehmite (γ–Al_2O_3, H_2O). Sc_2O_3 oxide forms on the upper part of the less defective aluminum oxy-hydroxide layers which increases the corrosion potential and decrease the rate of corrosion [22]. The presence

ISSN 1466-8858 Volume 12, Preprint 6 submitted 7 February 2009

of copper in the pits as revealed by EDS analysis (Figure 17-b) shows that copper particles are the preferred sites for attack. The presence of coherent nano-precipitates allows the formation of a highly homogeneous protective film which is a combination of oxy-hydroxides of aluminum and Sc_2O_3 which plays a leading role in suppression of corrosion. The corrosion resistance of Al-Mg-Sc-Zr alloys is dictated by coherent nano-structured precipitates and their tendency for passivation. Both mechanical properties and corrosion resistance are dictates by the geometry, size and coherency, and volume fracture of the nano-precipitates on the grain sizes. More work is needed to be done to determine the microcharacteristic and kinetic of the duplex aluminum oxy-hydroxides and Sc_2O_3 films and their microstructured properties.

CONCLUSIONS

On the basis of the experimental studies conducted on five Al-Mg alloys containing varying scandium addition with zirconium, the following conclusions are drawn:

1) A maximum increase in the yield strength was observed on adding 0.3% Sc. All scandium added alloys (0.15, 0.3, 0.6, and 0.9%) showed higher strength compared to scandium-free alloys.

2) TEM studies showed small coherent precipitates $Al_3(Sc_{x-1}\ Zr_x)$ with a large volume fraction. The nano precipitate showed an increase in diameter with increased Sc contents.

3) As shown by the TEM evidence of Orwans grain boundary strengthening is the largest contributor to the strength of Al-Mg-Sc alloys. The evidence of pinning of grain boundaries by nano-size precipitates is established.

ISSN 1466-8858 Volume 12, Preprint 6 submitted 7 February 2009

4) The experimental Al-Mg-Sc alloys investigated offer a promising potential for replacement of conventional Al 2024-T4, Al 6013-T4, and Al 6061-T1, in view of their structural, mechanical, and corrosion characteristics.

5) The scandium added alloys are fairly resistant to corrosion in 3.5 wt% NaCl as shown by electrochemical studies. Corrosion occurs by breakdown of the duplex aluminum hydroxide and scandium oxide film. The secondary phase particles of copper appears to be the initiation sites for breakdown.

6) No evidence of exfoliation and intergranular attack was observed. Corrosion occurs preferentially at the interface between the precipitates and the matrix of copper particles.

ACKNOWLEDGMENTS

The authors acknowledge the financial assistance provided by the Dean of Scientific Research, King Fahd University of Petroleum & Minerals, in this project. The valuable assistance provided by FEI, Enahoven, The Netherlands, in providing generous assistance in studies conducted by Quanta 3D FEC STEM.

REFERENCES

1. Valiev, R. Z., Islamgaliev, R. K., and Alexandrov, I. V., (2000), *Prog. Mater. Sc*., **45**, 103.

2. Skinner, D. J., Kim, Y. W., Griffith, W. M., Editors (1988), **Dispersion Strengthened Hardened Aluminum Alloys**, TMS Publishing, 18.

3. Leng, Y., Porr, W. C., and Gangloff, R. P., (1990), *Scripta Metal and Mat*., **24**. 2173/

4. Filatov, Y. A., Yelagin, V. I., and Zacharov, V. V., (2000), *Mat. Sc. Eng. A*., **280**, 97.

5. Toropova, L. S., Eskin, D. G., Kharaketorva, M. L., and Dobatkina, P. V., (1998), **Advanced Aluminum Alloys Containing Scandium**, Gordon and Breach.

ISSN 1466-8858 Volume 12, Preprint 6 submitted 7 February 2009

6. Kuny, Songruil, Wenxian, L., Yude, X., (1999), *Trans. Nonfer. Met. Soc. China*, **9**, 593.

7. Savagen, F., Dunbar, B. R., in (2000), **Automotive Alloys**, Das, S., (Editor), Warrendale, PA., TMS, 239.

8. Fuller, C. B., Krause, A. R., Dunand, D. C., and Seidman, D. N., (2002), *Mat. Sc. Eng. A*., **338**, 8.

9. Roder, O., Schaurete, O., Lutjering, G., and Gysler, A., (1996), *Mat. Sc. Forum*, **217**, 1835-1840.

10. Fuller, C. B., Seidman, D. N., and Dunand, D. C., (2003), *Acta Materialia*, **51**, 4803-4814.

11. Fazeli, F., Poole, W. J., and Sinclair, C. W., (2008), *Acta Materialia*, **56**, 1909-1918.

12. ASTM Designation D638, Recommended Practice for Tensile Testing, (2003), **ASTM Annual Standards**, Metals Park, Ohio, U.S.A.

13. ASTM G5-87, ASTM Practice for Making Potentiostatic and Potentiodynamic Polarization Measurement, (1998), **Annual Book of Standards**, Part 10, **03.02**, Metals Park, Ohio, U.S.A.

14. ASTM G59-91, ASTM Practice for Making Polarization Resistance Plots, (1998), **Annual Book of Standards**, Part 10, **03.02**, Metals Park, Ohio, U.S.A.

15. Neubert, V., Smola, B., Stulikova, L., et al. (2007), *Mat. Sc. And Eng. A*, **464**, 358-364.

16. McNelly, T. B., Lee, E. W., and Miller, M. E., (1986), *Metall. Trans. A*., **17A**, 1043-1050.

17. Ahmad, Z., Anwarul Hamid, and Abdul Aleem, B. J., (2001), *Corros. Sc*., **43**, 1227-1243.

18. Sawtell, R. R., and Jenson, C. L., (1990), *Metallurgical Transactions*, Feb., 426.

19. Sanders, T. H., (1980), Ludwiczak, E. A., and Sawtell, R. R., *Mater. Sc. Eng*., **43**, 247-260.

20. Kendig, K. L., and Miracle, D. B., (2002), *ActaMaterialia*, **50**, 4165-4175.

21. Ahmad, Z., and Abdul Aleem, B. J., (2005), KACST Final Report, King Abdulaziz City of Science and Technology, Riyadh, Saudi Arabia.

22. Sinyaskii, V. S., Yalkov, V. D., and Titkova, E. V., (1998), *Protection of Metals*, **34**(6).

ISSN 1466-8858 Volume 12, Preprint 6 submitted 7 February 2009

Table 1 – Composition of Al-Mg-Sc-Zr Alloys.

Sl. No.	Alloy Name	Si	Fe	Cu	Mn	Mg	Cr	Zn	Ti	Zr	Sc
1	Al-Mg-Zr 0.0-Sc 0.0	0.087	0.166	0.002	0.003	2.96	0.002	0.0025	0.03	–	–
2	Al-Mg-Zr 0.14-Sc 0.15	0.08	0.16	0.002	0.003	2.97	0.0014	0.006	0.024	0.14	0.15
3	Al-Mg-Zr 0.14-Sc 0.3	0.09	0.15	0.002	0.003	2.95	0.0013	0.010	0.024	0.14	0.3
4	Al-Mg-Zr 0.14-Sc 0.6	0.1	0.16	0.002	0.003	2.96	0.001	0.002	0.021	0.14	0.6
5	Al-Mg-Zr 0.14-Sc 0.9	0.092	0.16	0.003	0.004	2.87	0.001	0.007	0.028	0.14	–

Table 2 – Mechanical Properties of Al-2.5 Mg Alloys with and without Scandium.

Alloy	0.2% P.S.	UTS
Al-2.5 Mg	130	202
Al-2.5 Mg + 0.3 Sc	255.3	319

Table 3 – Mechanical Properties of Al-Mg-Sc-Zr Alloys at Room Temperature.

Sl. No.	Alloy	Ultimate Tensile Strength (MPa)	% Fracture Strain	Modulus (GPa)	Yield Strength (MPa)	% Elongation
1	Alloy 1	198	15.52	50	123.4	14
2	Alloy 2	248	11.88	58	210.2	9.5
3	Alloy 3	319	18.21	56	255.3	9.0
4	Alloy 4	288	15.77	76	214.5	8.5
5	Alloy 5	280	11.28	56	201.8	7.5

The yield strength after aging of alloy 3 for 100 hours at 300°C was 248 MPa.

ISSN 1466-8858 Volume 12, Preprint 6 submitted 7 February 2009

Table 4 – Electrochemical Parameters of Alloys obtained by Polarization Resistance Measurements.

Alloy Type	R_p (k-Ohms)	E (I = 0) (mV)	I_{corr} (uA)	β_a (V/dec.)	β_c (V/dec.)	Corrosion Rate (mpy)	Corrosion Rate (mm/yr)
Alloy 1	1.392	–782.0	16.98	82.32 E – 3	160.8 E – 3	7.284	0.185
Alloy 2	1.635	802.6	14.84	86.91 E – 3	156.3 E – 3	6.365	0.162
Alloy 3	1.837	–765.5	14.29	85.14 E – 3	208.5 E – 3	6.130	0.156
Alloy 4	1.230	–793.9	15.55	69.40 E – 3	120.5 E – 3	6.671	0.169
Alloy 5	1.289	–794.5	17.06	79.36 E – 3	139.9 E – 3	7.316	0.186

Table 5 – Cyclic Polarization of Al-Mg-Zr Alloys.

Sl. No.	Alloy	Sc (%)	E_p (V)	E_{pp} (V)	E_{corr} (V)	$E_1 = E_p - E_{corr}$
1	Alloy 1	0	–0.715	–0.783	–0.84	0.127
2	Alloy 2	0.15	–0.721	–0.795	–0.786	0.065
3	Alloy 3	0.3	–0.701	–0.812	–0.758	0.057
4	Alloy 4	0.6	–0.755	–0.803	–0.826	0.071
5	Alloy 5	0.9	–0.766	–0.811	–0.848	0.082

ISSN 1466-8858 Volume 12, Preprint 6 submitted 7 February 2009

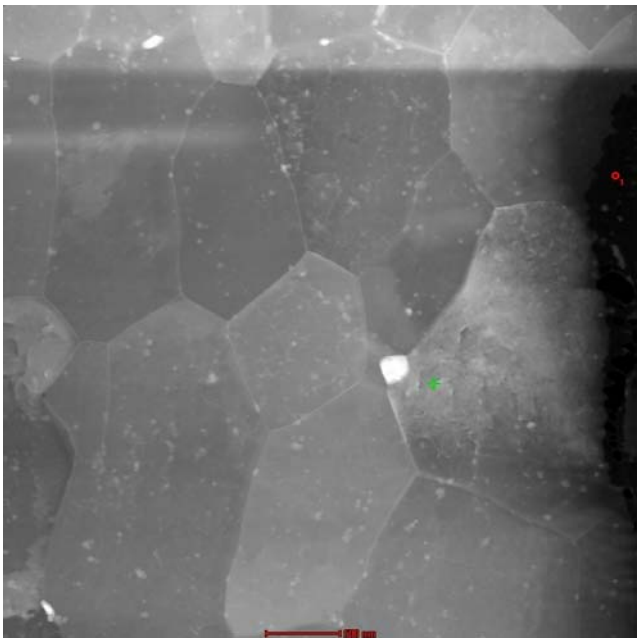

Figure 1 – A FEGSTEM (DF) image of alloy containing 0.3 Sc and 0.15 Zr. The image shows the sub-grains and nano-precipitates.

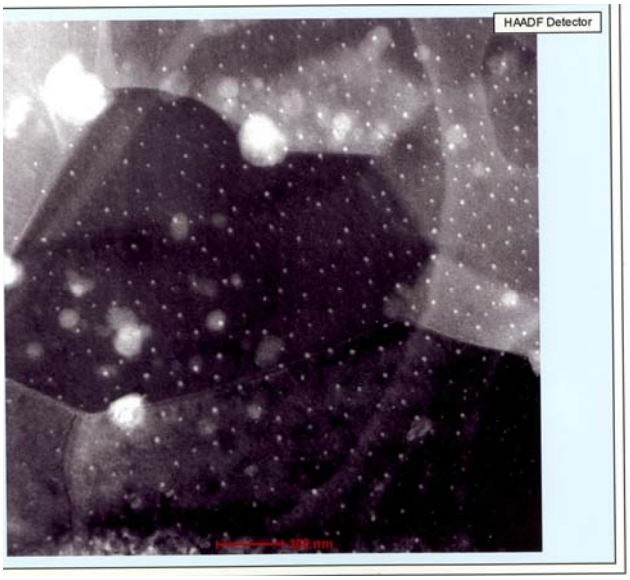

Figure 2 – A HAADF-STEM image shows coherent distribution of nano-precipitates.

ISSN 1466-8858 Volume 12, Preprint 6 submitted 7 February 2009

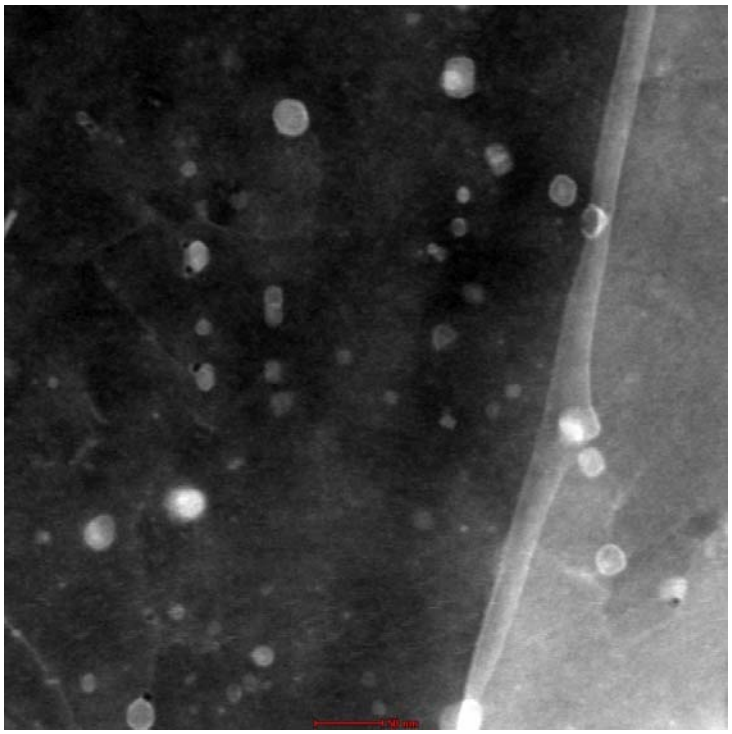

Figure 3 – A FEGSTEM (DF) image shows the grain boundaries and the precipitates.

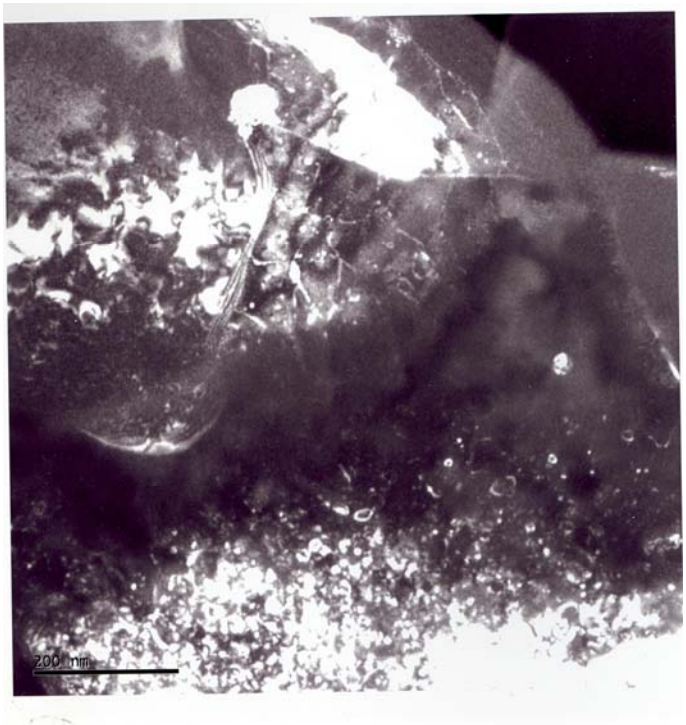

Figure 4 – Dark field image showing dislocations at the grain boundaries.

ISSN 1466-8858 Volume 12, Preprint 6 submitted 7 February 2009

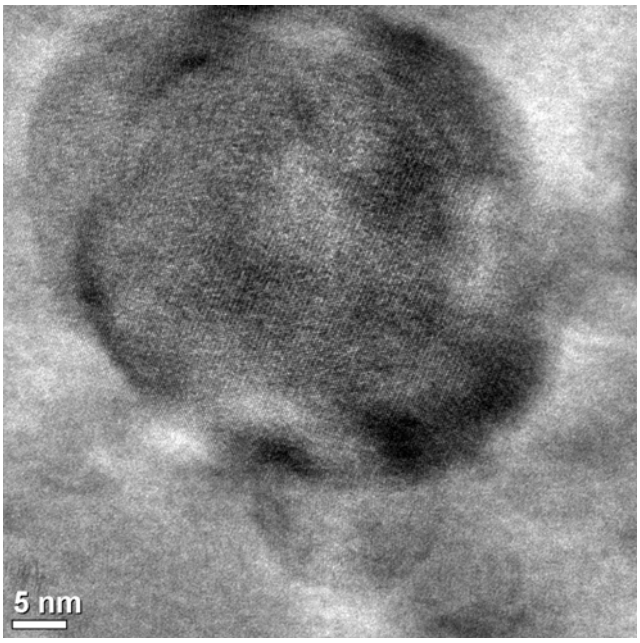

Figure 5 – A HRTEM image of alloy containing 0.3 Sc and 0.15 Zr showing the coherency of the precipitates of $Al_3(Sc_{x-1}\text{-}Zr_x)$.

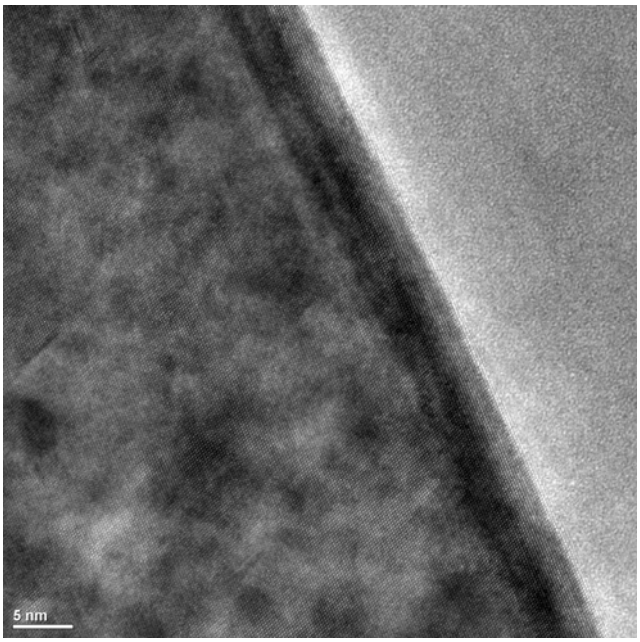

Figure 6 – A HRTEM image of alloy containing 0.3 Sc and 0.15 Zr showing grain boundary interface.

ISSN 1466-8858 Volume 12, Preprint 6 submitted 7 February 2009

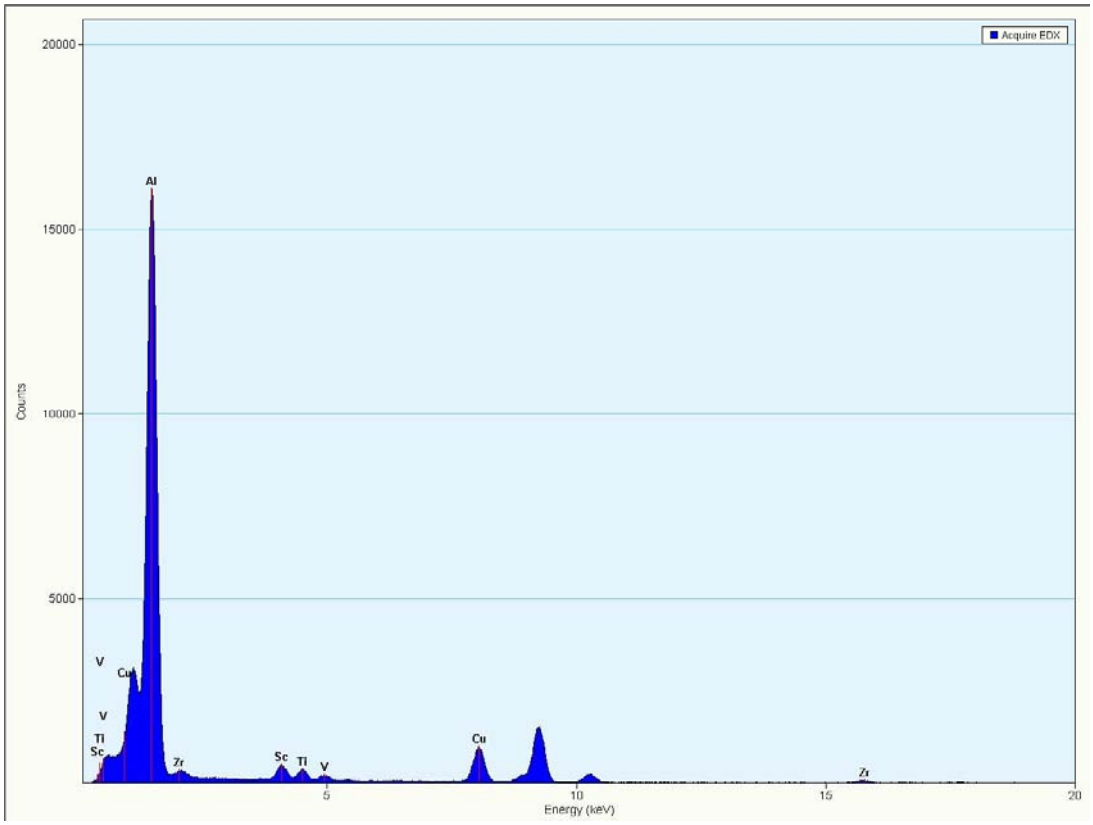

Figure 7 – EDS analysis of alloy containing 0.3 Sc and 0.15 Zr.

ISSN 1466-8858 Volume 12, Preprint 6 submitted 7 February 2009

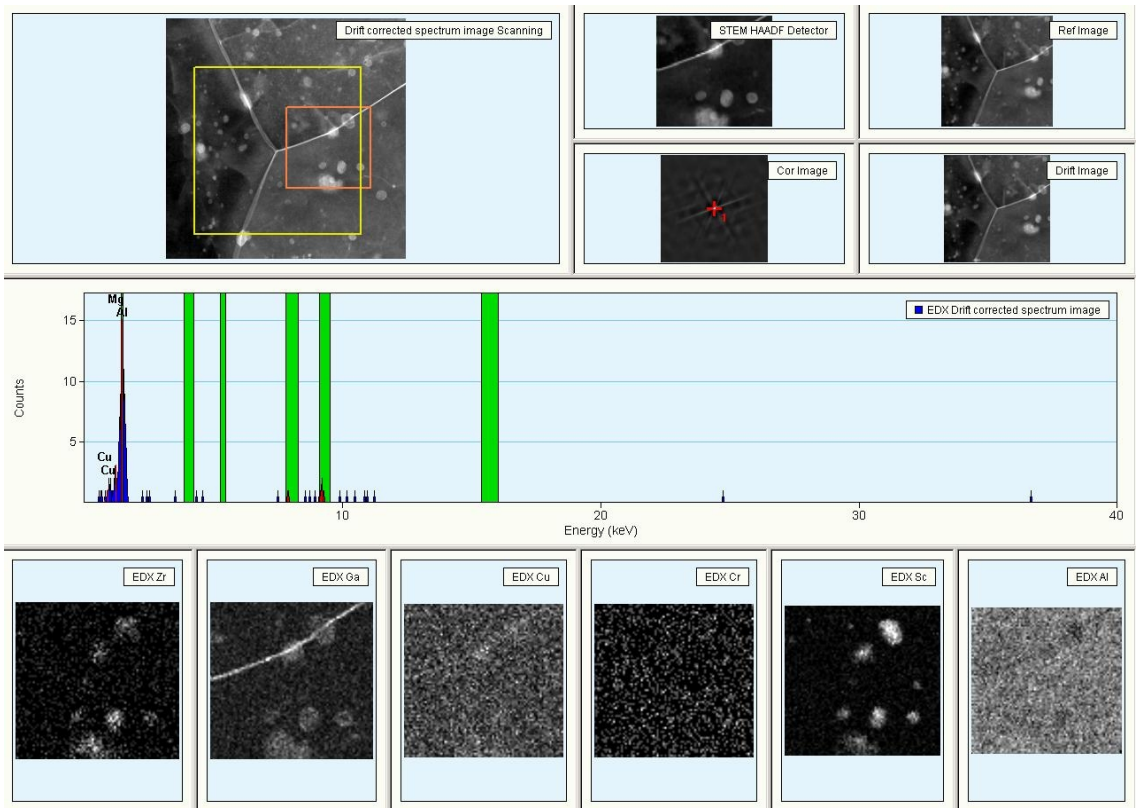

Figure 8 – EDS mapping of alloy containing 0.3 Sc and 0.5 Zr.

ISSN 1466-8858 ıbmitted 7 February 2009

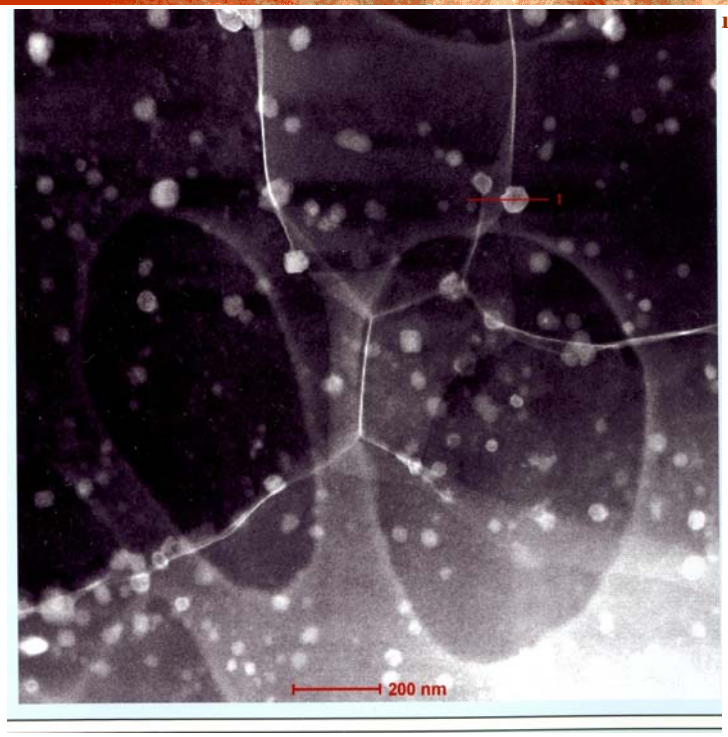

Figure 9 – A HAADF-STEM image showing the pinning of the grain boundaries by the precipitates.

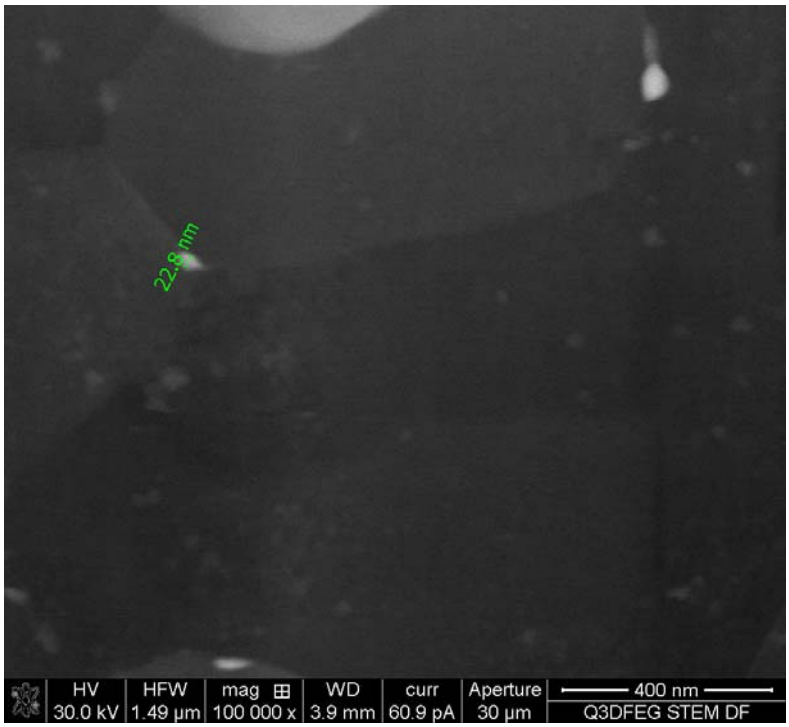

Figure 10 – A quantum 3D FEGSTEM image of precipitates showing the size of nano-particles.

ISSN 1466-8858 Volume 12, Preprint 6 submitted 7 February 2009

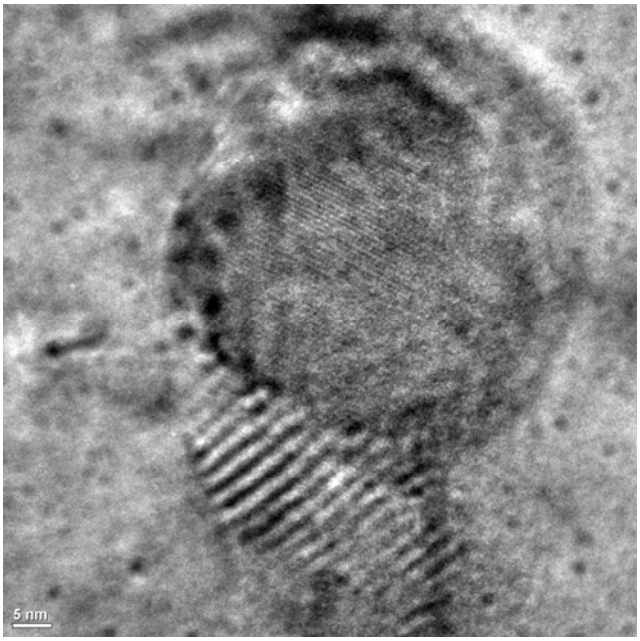

Figure 11 – A HRTEM image showing homogeneously distributed precipitates.

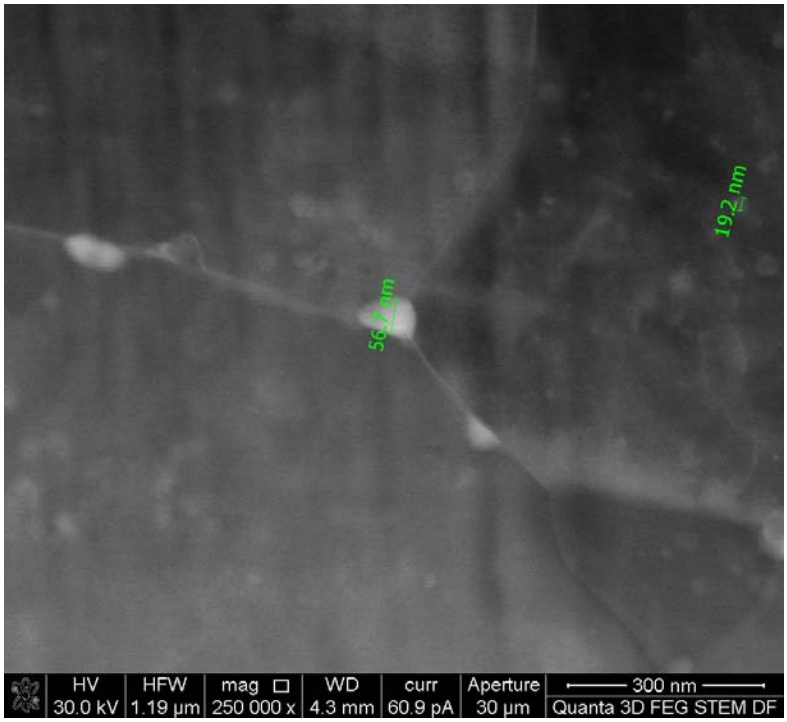

Figure 12 – Nano-precipitates ranging from 19.2 nm to 56.7 nm in alloy containing 0.6 Sc.

ISSN 1466-8858 Volume 12, Preprint 6 submitted 7 February 2009

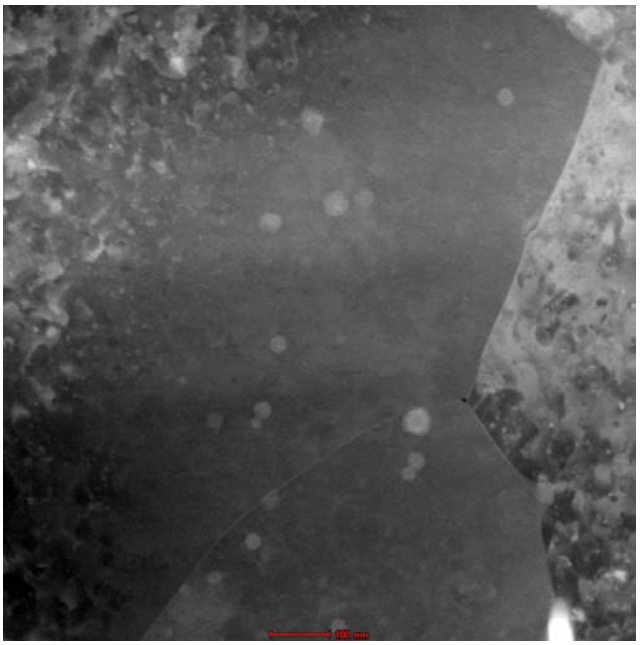

Figure 13 – A FEGSTEM image showing dislocations and the precipitates at the grain boundaries.

Figure 14-a – Dislocation loop at the grain boundaries in alloy containing 0.9% Sc.

ISSN 1466-8858 Volume 12, Preprint 6 submitted 7 February 2009

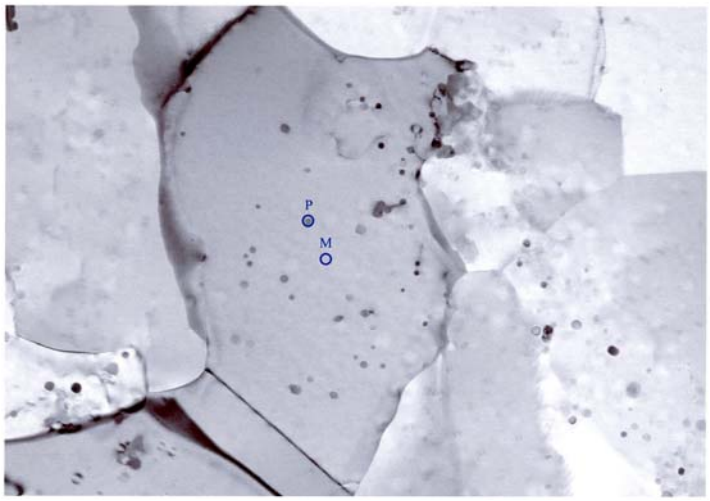

Figure 14-b – Dislocation loop at the grain boundary in alloy containing 0.9% Sc.

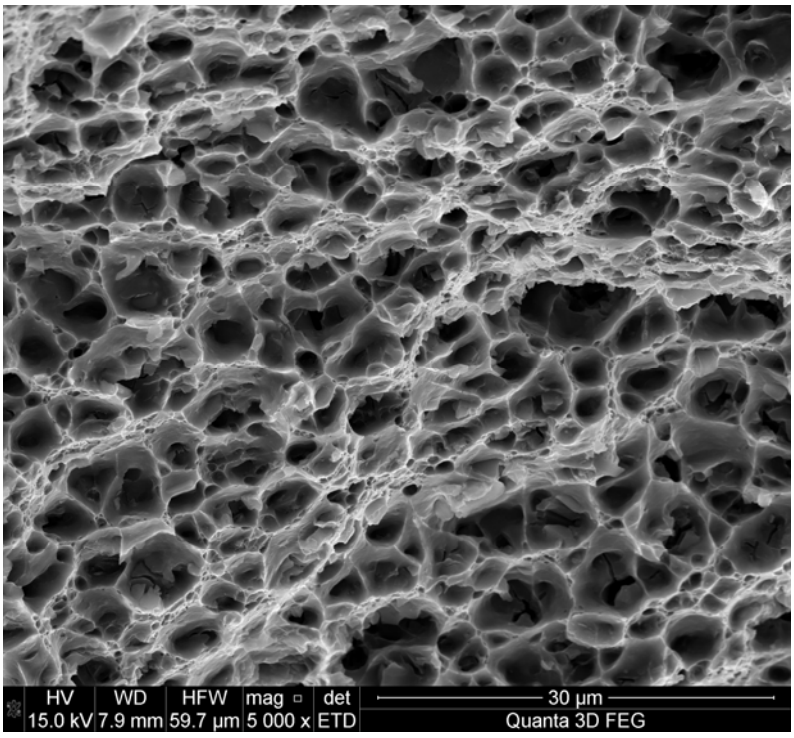

Figure 15 – A FEGSTEM image of dimpled surface of alloy containing 0.6% Sc.

ISSN 1466-8858 Volume 12, Preprint 6 submitted 7 February 2009

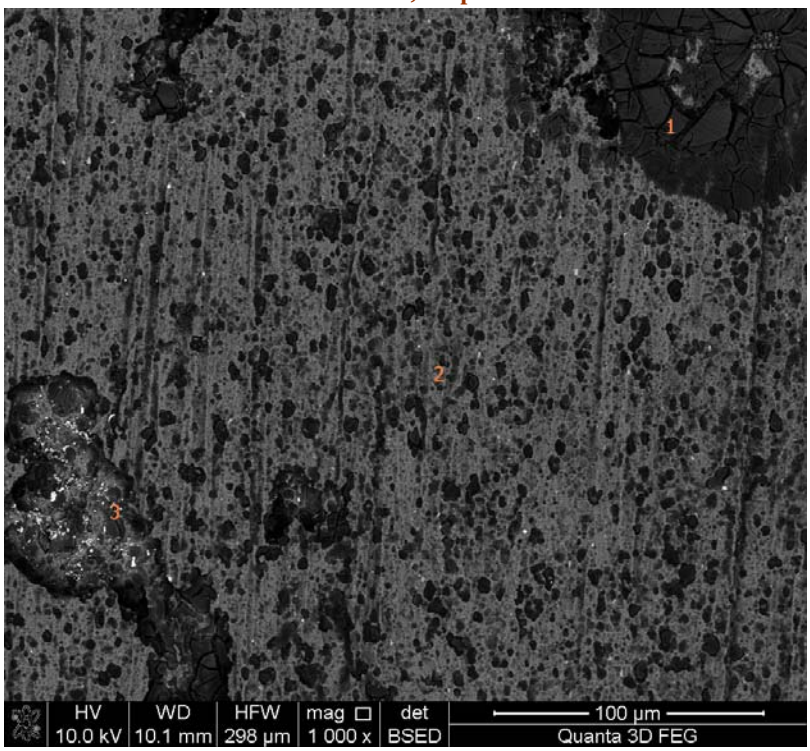

Figure 16-a – The surface of alloy containing 0.3 Sc and 0.15 Zr showing the sites of preferred attack.

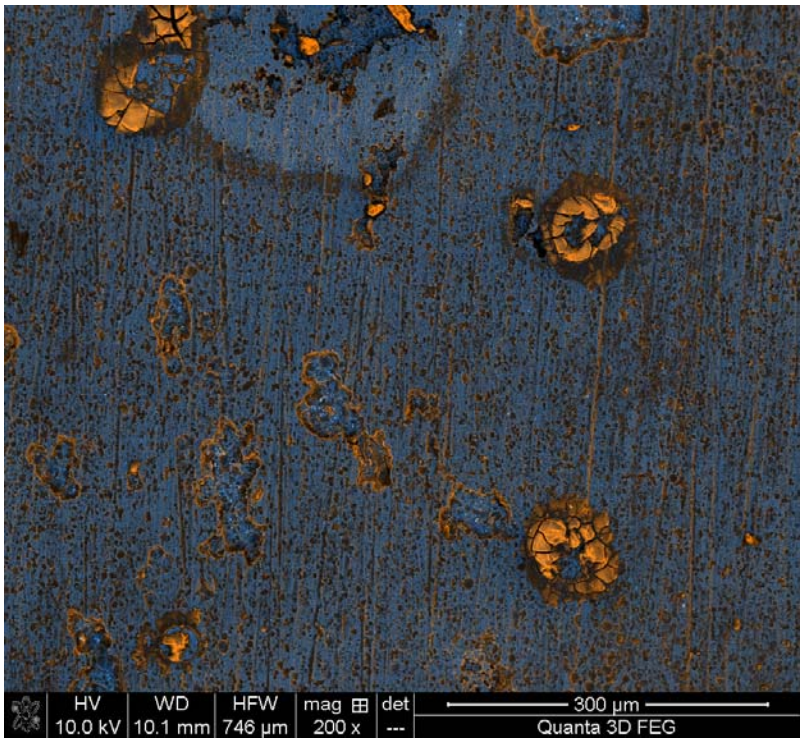

Figure 16-b – Interspace and the precipitates on intermetallic particles.

ISSN 1466-8858 itted 7 February 2009

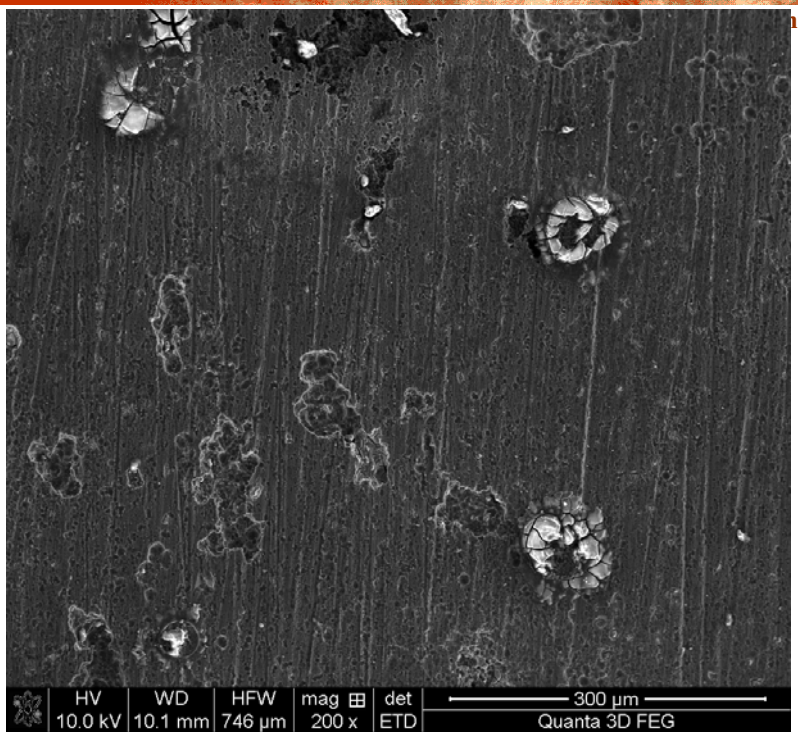

Figure 17-a – The high copper peaks indicate the presence of copper (white particles) on the preferred sites for corrosion.

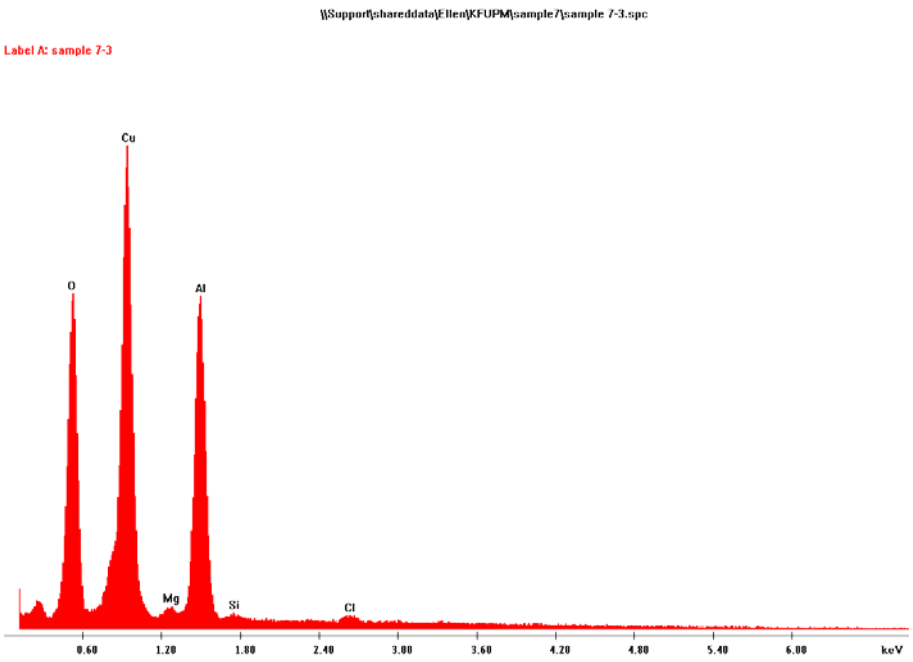

Figure 17-b – EDS spectra of a copper-rich site.

ISSN 1466-8858 Volume 12, Preprint 6 submitted 7 February 2009

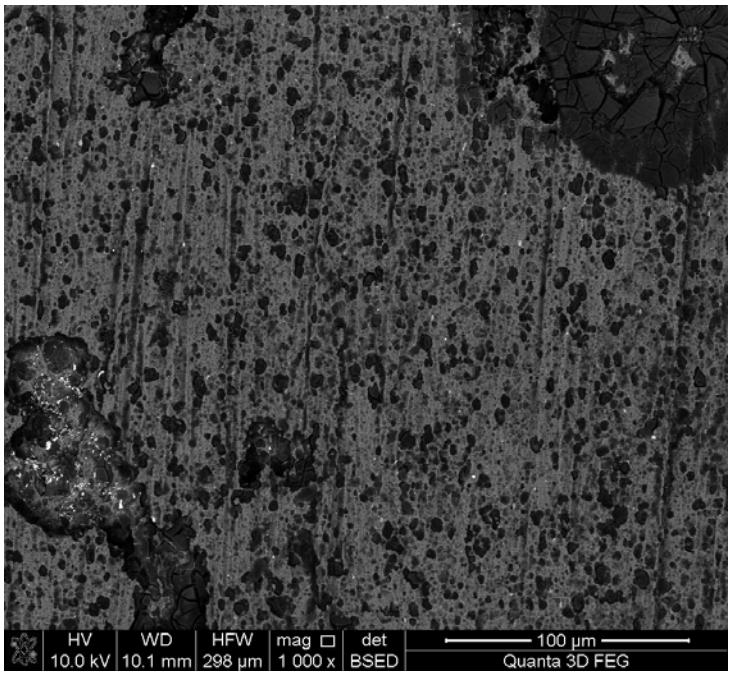

Figure 18 – FEGSTEM image of a corroded sample showing breakdown of the oxide layer (right-hand corner) and corrosion around the agglomerates of nano-particles.